

Research Article

An Areal Assessment of Subseafloor Carbon Cycling in Cold Seeps and Hydrate-Bearing Areas in the Northern South China Sea

Yanping Zhang ¹, Min Luo ^{2,3}, Yu Hu,³ Hongbin Wang,⁴ and Duofu Chen ^{1,3}

¹State Key Laboratory of Isotope Geochemistry, Guangzhou Institute of Geochemistry, Chinese Academy of Sciences, Guangzhou 510640, China

²Laboratory for Marine Geology, Qingdao National Laboratory for Marine Science and Technology, Qingdao 266061, China

³Shanghai Engineering Research Center of Hadal Science and Technology, College of Marine Sciences, Shanghai Ocean University, Shanghai 201306, China

⁴Guangzhou Marine Geological Survey, Guangzhou 510740, China

Correspondence should be addressed to Min Luo; mluo@shou.edu.cn and Duofu Chen; dfchen@shou.edu.cn

Received 25 November 2018; Accepted 20 January 2019; Published 17 March 2019

Academic Editor: Giovanni Martinelli

Copyright © 2019 Yanping Zhang et al. This is an open access article distributed under the Creative Commons Attribution License, which permits unrestricted use, distribution, and reproduction in any medium, provided the original work is properly cited.

Gas hydrates, acting as a dynamic methane reservoir, store methane in the form of a solid phase under high-pressure and low-temperature conditions and release methane through the sediment column into seawater when they are decomposed. The seepage of methane-rich fluid (i.e., cold hydrocarbon seeps) fuels the chemosynthetic biota-inhabited surface sediments and represents the major pathway to transfer carbon from sediments to the water column. Generally, the major biogeochemical reactions related to carbon cycling in the anoxic marine sediments include organic matter degradation via sulfate reduction (OSR), anaerobic oxidation of methane (AOM), methanogenesis (ME), and carbonate precipitation (CP). In order to better understand the carbon turnover in the cold seeps and gas hydrate-bearing areas of the northern South China Sea (SCS), we collected geochemical data of 358 cores from published literatures and retrieved 37 cores and corresponding pore water samples from three areas of interest (i.e., Xisha, Dongsha, and Shenhu areas). Reaction-transport simulations indicate that the rates of organic matter degradation and carbonate precipitation are comparable in the three areas, while the rates of AOM vary over several orders of magnitude (AOM: 8.3–37.5 mmol·m⁻²·yr⁻¹ in Dongsha, AOM: 12.4–170.6 mmol·m⁻²·yr⁻¹ in Xisha, and AOM: 9.4–30.5 mmol·m⁻²·yr⁻¹ in Shenhu). Both the arithmetical mean and interpolation mean of the biogeochemical processes were calculated in each area. Averaging these two mean values suggested that the rates of organic matter degradation in Dongsha (25.7 mmol·m⁻²·yr⁻¹) and Xisha (25.1 mmol·m⁻²·yr⁻¹) are higher than that in Shenhu (12 mmol·m⁻²·yr⁻¹) and the AOM rate in Xisha (135.2 mmol·m⁻²·yr⁻¹) is greater than those in Dongsha (27.8 mmol·m⁻²·yr⁻¹) and Shenhu (17.5 mmol·m⁻²·yr⁻¹). In addition, the rate of carbonate precipitation (32.3 mmol·m⁻²·yr⁻¹) in Xisha is far higher than those of the other two regions (5.3 mmol·m⁻²·yr⁻¹ in Dongsha, 5.8 mmol·m⁻²·yr⁻¹ in Shenhu) due to intense AOM sustained by gas dissolution. In comparison with other cold seeps around the world, the biogeochemical rates in the northern SCS are generally lower than those in active continental margins and special environments (e.g., the Black sea) but are comparable with those in passive continental margins. Collectively, ~2.8 Gmol organic matter was buried and at least ~0.82 Gmol dissolved organic and inorganic carbon was diffused out of sediments annually. This may, to some extent, have an impact on the long-term deep ocean carbon cycle in the northern SCS.

1. Introduction

Marine sediments are the Earth's largest methane reservoir, in which methane is dominantly preserved as gas hydrates that are commonly distributed along continental margins [1, 2]. It is estimated that at least 600 Gt methane is stored

as hydrates in the continental margin sediments characterized by relatively high-pressure and low-temperature conditions [3]. However, as a dynamic methane reservoir, gas hydrates tend to decompose when the equilibrium state breaks, potentially leading to ocean acidification, submarine slope instability, and global climate change [2–4]. In

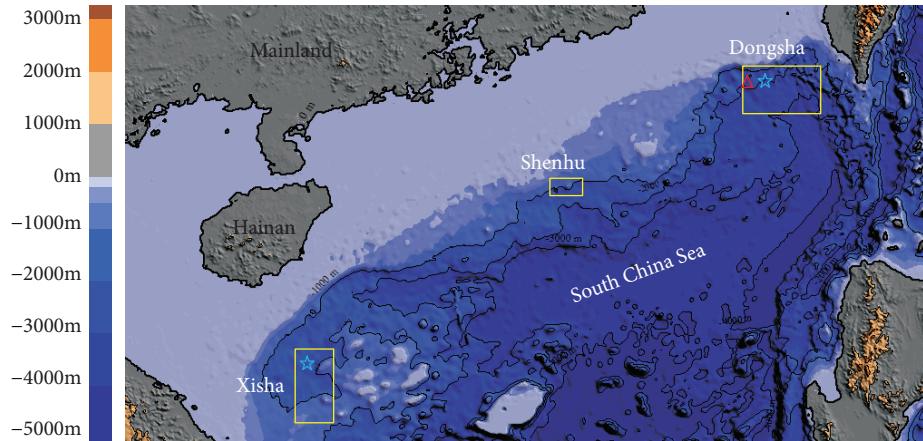


FIGURE 1: The bathymetric map of the northern South China Sea. Rectangle boxes denote study areas. Note that Xisha herein includes the Qiongdongnan basin and Xisha Uplift, and Dongsha comprises a broad area of the eastern Zhujiangkou basin and SW Taiwan basin. The blue stars denote active seepage sites. The red triangle represents the Jiulong methane reef covering an area of $\sim 400 \text{ km}^2$.

addition, in light of the resource potential and environmental effect, gas hydrate has drawn increasing attentions worldwide since its first discovery in 1970s.

Gas hydrates are usually closely coupled with cold seeps at continental slopes. On the continental margins, methane produced through either microbial methanogenesis or pyrolysis of organic matter can precipitate as hydrates when the dissolved methane concentration exceeds methane hydrate solubility within the gas hydrate stability zone [2, 5–7]. The gas hydrates will decompose and release large amounts of methane into the water column upon the pressure and/or temperature changes induced by global warming and sea level changes. The migration of methane-rich fluid towards the seafloor forms the cold seeps and associated seafloor expressions (e.g., mound or crater-like shape) [8]. Globally, the vast majority of methane in the sediments is consumed by the anaerobic oxidation of methane (AOM) mediated by anaerobic methane-oxidizing archaea and sulfate-reducing bacteria [9, 10]. AOM thus represents a microbial filter largely preventing dissolved methane from escaping the sediments. In the intensive seepage areas, a large amount of methane is usually transported in a gas phase as bubble, which cannot be fully consumed by AOM. The main product of AOM, dissolved inorganic carbon (DIC), can either precipitate as authigenic carbonate or migrate towards the seafloor. Other DIC sources in the sediments include organoclastic sulfate reduction and methanogenesis, which also makes important contribution to the DIC reservoir.

The South China Sea (SCS), as one of the major marginal seas around the west Pacific Ocean, is well known for its extensive distribution of high-saturation gas hydrate [11–14]. Since the 1990's, high-resolution seismic surveys have been carried out to delineate the distribution of bottom-simulating reflectors (BSR) and determine the prospecting area of gas hydrates. Through several hydrate survey expeditions, six promising hydrate-bearing areas including Dongsha, SW Taiwan, Xisha, Qiongdongnan, Shenhu, and Beikang have been confirmed to date [13–20]. Besides, more than 40 cold seepage sites have been indicated by

the occurrence of ^{13}C -depleted authigenic carbonate and seep-associated fauna and anomalous pore water and sediment geochemistry influenced by fluid seepage [6, 21–25]. Several pioneering studies have targeted at quantifying the rate of biogeochemical reactions and carbon fluxes at the seafloor using the reaction-transport model, in the specific seep sites of the northern SCS [16, 24, 26, 27]. Nevertheless, our quantitative understanding of the subsurface carbon cycle on a regional scale still remains limited. Therefore, the area-based carbon cycle calls for sufficient geochemical data combined with the numerical modeling approach to understand the relationship among different carbon reservoirs and their potential impact on the seawater carbonate system. In this study, 37 sediment cores were collected from the Shenhu area, Dongsha area, and Xisha area. The 1-D reaction-transport model was subsequently applied to quantify site-specific rates of biogeochemical processes and fluxes of DIC and methane. In combination with 358 published cores from the areas of interest, spatial interpolation was then used to explore the regional distribution of biogeochemical rates in the three regions. Finally, the areal assessments of surface carbon cycling in the northern SCS were provided to reveal the relationship among different carbon inventories.

2. Study Area

The SCS formed in the late Jurassic-early Cretaceous is located at the confluence of three plate collision, including the Pacific plate, Eurasia plate, and India-Australia plate [28]. The northern margin is a typical passive continental setting with a broad shelf, which is bounded to the west by the Indochina peninsula and to the east by a chain of island arcs [28]. The study area includes three areas in the northern slope of the SCS (Xisha, Shenhu, and Dongsha), with the water depth ranging from ~ 700 to ~ 2000 meters (see Figure 1). All these regions unanimously have experienced two tectonic stages, i.e., the syn-rift stage during the Paleocene and Oligocene and post-rift stage [29]. The infill of the northern continental marginal basins evolved simultaneously

from alluvial and lacustrine deposits to neritic deposits, followed by progradational packages of slope sediments [30]. The lacustrine sediments deposited in the depressions acted as important source rocks for hydrocarbon generation. The potential abundant gas hydrate reservoirs have been indicated by the widespread occurrence of bottom-simulating reflectors (BSRs) [12, 31] (see Figure 1). The gas hydrates, retrieved by GMGS1&3 hydrate-drilling expeditions conducted by the Guangzhou Marine Geology Survey at the water depth of ~2000 meters in the Shenhu area, are characterized by a high-saturation (up to 40%) and mixed gas source [12]. During the GMGS2 hydrate-drilling expedition in Dongsha, various gas hydrate morphologies including massive, fracture-filling, and disseminated hydrates were found in the collected cores [31]. In addition, active seepage sites were discovered during remotely operated vehicle (ROV) deployments in the Dongsha and Xisha areas [21, 32]. These active seepage sites are characterized by the existence of gas ebullition in the water column; living chemosynthesis-based communities, such as mussels, tubeworms, and clams; and abundant authigenic carbonate rocks in the form of crusts, nodules, and tubular concretion.

3. Sampling and Methods

3.1. Sampling. In total, the 37 sediment cores used in this study were collected from five expeditions by using different research vessels. Four cores were retrieved by gravity corers from the Dongsha area during the Haiyang-4 cruise conducted by the Guangzhou Marine Geological Survey in October 2013. The sediments consisted of homogeneous green-gray clay silt, embedded by several small authigenic carbonate nodules. The Dongsha area was visited twice by Shiyang-3 in April 2014 and by Haiyang-4 in May 2015. The sediments were sampled by piston-gravity corers and box corers. In the Xisha area, five piston cores were retrieved by Haiyang-4 in April 2015. The sediments change from brown silt clay to gray calcareous clay. Twenty-four cores in Shenhu were collected by piston corer using Haiyang-4 in May 2015 and September 2016. The lithology in the Shenhu area was similar to that in the Xisha area, consisting of brown to gray calcareous silt. Detailed information with regard to core lengths, water depths, and sampling gears were shown in Table S1. All the retrieved cores were immediately brought to the onboard laboratory for porewater extraction. Rhizon samplers were used to collect porewater at 20 cm or 40 cm intervals. Porewater aliquots were stored at 4°C with ultrapure concentrated HNO₃ and saturated HgCl₂ solution for anion and cation analyses, respectively.

3.2. Analytical Methods. Concentrations of total alkalinity (TA) and phosphate (PO₄³⁻) were measured onboard immediately after pore water collection. The TA concentrations were determined by direct titration with 0.006 M HCl using Bruevich's method [33]. The analysis was calibrated using standard seawater (IAPSO) with a precision of better than 2%. Phosphate concentrations were determined using a HITACHI U-5100 spectrophotometer with the analytical

precision of better than 5%. Concentrations of sulfate (SO₄²⁻), chloride (Cl⁻), and calcium (Ca²⁺) were determined onshore by a Dionex ICS-5000+ ion chromatography at the South China Sea Institute of Oceanology, Chinese Academy of Sciences (CAS), with the analytical precision better than 2%. Dissolved inorganic carbon (DIC) concentrations were measured by an IsoPrime 100 continuous flow isotope ratio mass spectrometer (CF-IRMS) at the State Key Laboratory of Isotope Geochemistry, Guangzhou Institute of Geochemistry, CAS, with the precision of better than 2%. Detailed analytical processes can be found in the study of Hu et al. [34].

3.3. Reaction-Transport Modeling. A one-dimensional, steady-state, reaction-transport model developed from previous approaches was applied to simulate one as a solid phase (POC) and five as dissolved species (SO₄²⁻, CH₄, DIC, Ca²⁺, and PO₄³⁻). Two partial differential equations were used to reproduce the depth concentration profiles of solid and dissolved species [35–37].

$$\phi \frac{\partial C_a}{\partial t} = \frac{\partial(\phi \cdot D_s \cdot (\partial C_a / \partial x))}{\partial x} - \frac{\partial(\phi \cdot v_p \cdot C_a)}{\partial x} + \phi \cdot \sum R + \phi \cdot R_{\text{Bui}}, \quad (1)$$

$$(1 - \phi) \frac{\partial \text{POC}}{\partial t} = - \frac{\partial((1 - \phi) \cdot v_s \cdot \text{POC})}{\partial x} + (1 - \phi) \cdot \sum R, \quad (2)$$

where t (year) is time, x (cm) is depth below the seafloor, ϕ (dimensionless) is porosity, D_s (cm²·yr⁻¹) is solute-molecular diffusion coefficient corrected by tortuosity, C_a (mol/L) is the concentrations of solutes in pore water, POC (wt.%) is the content of POC in dry sediment, v_p (cm·yr⁻¹) is the burial velocity of porewater due to steady-state compaction, v_s (cm·yr⁻¹) is burial velocity of solid, $\sum R$ is the sum of rates of all chemical reactions considered in the model, and R_{Bui} is the mixing rate of bottom water and porewater due to bubble irrigation.

Sediment porosity decreases with depth assuming steady-state compaction. v_p and v_s are variables changing with porosity under assumption of steady-state compaction. Equations can be described as follows:

$$\phi = \phi_f + (\phi_0 - \phi_f) \cdot e^{-px}, \quad (3)$$

where ϕ_f (dimensionless) is the porosity at depth and ϕ_0 (dimensionless) is the porosity at the sediment-water interface. p (cm⁻¹) denotes the attenuation coefficient of porosity.

In the absence of externally imposed fluid advection at the seafloor, the velocity of porewater and solids is directed downward under steady-state compaction relative to the seafloor:

$$v_p = \frac{\phi_f \cdot w}{\phi},$$

$$v_s = \frac{(1 - \phi_f) \cdot w}{(1 - \phi)},$$
(4)

where w ($\text{cm}\cdot\text{yr}^{-1}$) is the sedimentation velocity.

Calibration of diffusive coefficient with tortuosity was after the equation of Boudreau [36].

$$D_s = \frac{D_m}{1 - \ln(\phi)^2},$$
(5)

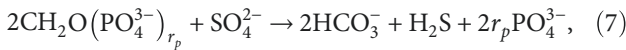
where D_m ($\text{cm}^2\cdot\text{yr}^{-1}$) is molecular diffusion coefficient in the in situ temperature, salinity, and pressure calculated according to Li and Gregory [38].

In sites 2015XS-R2 and 2015XS-50, gas ebullition during the ROV deployment was observed [32]. The porewater mixing with bottom water induced by rising gas bubbles can be described as a nonlocal transport similar to bioirrigation [39]:

$$R_{\text{Bui}} = \alpha_0 \cdot \frac{\exp(L_{\text{irr}} - x/\alpha_1)}{1 + \exp(L_{\text{irr}} - x/\alpha_1)} \cdot (C_0 - C_l),$$
(6)

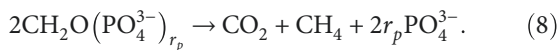
where α_0 (yr^{-1}) is the coefficient of irrigation intensity, L_{irr} (cm) is the depth of bubble irrigation, α_1 (cm) is the parameter determining how quickly bubble irrigation is attenuated to zero at an approximate depth of L_{irr} , C_0 is solute concentration at the SWI, and C_l is concentration at any depth within the irrigation zone.

As for biogeochemical reactions, organic matter decomposition via sulfate (OSR), methanogenesis (ME), anaerobic oxidation of methane (AOM), and authigenic carbonate precipitation (CP), as well as methane gas dissolution in a shallow hydrate-bearing site, are included in the model. Aerobic respiration, denitrification, manganese reduction, and iron reduction via organic matter remineralization were not taken into account in the model since these reactions were only restricted to the uppermost sediments (about 10-20 cm below the seafloor). Below the oxic and suboxic zones, sulfate serves as the main terminal electron acceptor for oxidizing organic matter [40–43]. Organic matter degradation via sulfate reduction was expressed as follows:



where r_p is the Redfield ratio of organic phosphorus to organic carbon.

Below the sulfate reduction zone, the organic matter was degraded via methanogenesis:



The rates of sulfate reduction and methanogenesis depend on the total rate of POC degradation according to Middelburg [44] and Wallmann et al. [37]:

$$R_{\text{POC}} = \frac{K_c}{[\text{DIC}] + [\text{CH}_4] + K_c} \cdot \left(0.16 \cdot \left(a_0 + \frac{x}{w}\right)^{-0.95}\right) \cdot \text{POC},$$
(9)

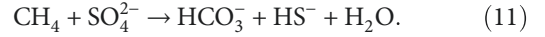
where K_c (M) is an inhibition coefficient of POC degradation, $[\text{DIC}]$ and $[\text{CH}_4]$ (mM) are concentrations of DIC and CH_4 , respectively, and a_0 (yr) is the initial age of organic matter, which was constrained using measured PO_4^{3-} concentrations. The rates of OSR and ME are thus expressed using the following equations:

$$R_{\text{OSR}} = 0.5 \cdot \frac{\rho_s \cdot (1 - \phi) \cdot 10^6}{\text{MW}_c \cdot \phi} \cdot \frac{[\text{SO}_4^{2-}]}{[\text{SO}_4^{2-}] + K_{\text{SO}_4^{2-}}} \cdot R_{\text{POC}},$$

$$R_{\text{ME}} = 0.5 \cdot \frac{\rho_s \cdot (1 - \phi) \cdot 10^6}{\text{MW}_c \cdot \phi} \cdot \frac{K_{\text{SO}_4^{2-}}}{[\text{SO}_4^{2-}] + K_{\text{SO}_4^{2-}}} \cdot R_{\text{POC}},$$
(10)

where ρ_s ($\text{g}\cdot\text{cm}^{-3}$) is the density of dry sediments, MW_c ($\text{g}\cdot\text{mol}^{-1}$) is the molecular weight of carbon, and $K_{\text{SO}_4^{2-}}$ is the Michaelis-Menten constant for the inhibition of sulfate concentration.

The AOM-coupled sulfate reduction mediated by a syntrophic consortium of methanotrophic archaea and sulfate-reducing bacteria is an important sink for methane in anoxic marine sediments [9, 45].

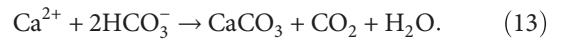


The rate of AOM was calculated using bimolecular kinetics:

$$R_{\text{AOM}} = k_{\text{AOM}} \cdot [\text{SO}_4^{2-}] \cdot [\text{CH}_4],$$
(12)

where k_{AOM} ($\text{cm}^3\cdot\text{mol}^{-1}\cdot\text{yr}^{-1}$) is an apparent second-order rate constant.

The DIC produced by AOM and organic matter degradation can be consumed due to precipitation of authigenic carbonate [35, 46, 47]:



The rate of authigenic carbonate precipitation was simulated using the thermodynamic solubility constant as defined by Millero [48]:

$$R_{\text{CP}} = k_{\text{CP}} \cdot \left(\frac{[\text{Ca}^{2+}] \cdot [\text{CO}_3^{2-}]}{K_{\text{SP}}} - 1 \right),$$
(14)

where k_{CP} ($\text{mol}\cdot\text{cm}^{-3}\cdot\text{yr}^{-1}$) is the kinetic constant and K_{SP} ($\text{mol}^2\cdot\text{l}^2$) is the thermodynamic equilibrium constant. A typical porewater pH value of 7.6 was used to calculate CO_3^{2-} from modeled DIC concentration [49]. CaCO_3 is not simulated explicitly in the model.

At sites 2015XS-R2, 2015XS-50 where gas ebullition was observed, dissolution of rising gas bubble occurs if the

porewater is undersaturated with respect to in situ methane gas solubility:



where L_{MB} (mol/L) is a site-specific constant dependent on in situ salinity, pressure, and temperature using the algorithm in the work of Duan et al. [7, 50]. The rate of gas dissolution was described using a first-order kinetic expression of the departure from the local methane gas solubility concentration:

$$R_{\text{MB}} = k_{\text{MB}} \cdot (L_{\text{MB}} - [\text{CH}_4]), \quad (16)$$

where k_{MB} (yr^{-1}) is a first-order rate constant.

Gas hydrate precipitation occurred if the dissolved methane concentration exceeded the solubility of gas hydrate (L_{GH}):

$$R_{\text{GH}} = k_{\text{GH}} \cdot \left(\frac{[\text{CH}_4]}{L_{\text{GH}}} - 1 \right), \quad (17)$$

where k_{GH} ($\text{mol}\cdot\text{cm}^{-3}\cdot\text{yr}^{-1}$) is a fitting parameter constrained by the depth of the first occurrence of gas hydrate.

Upper and lower boundary conditions for all species were imposed as fixed concentrations with the exception of the intensive seepage site (2015XS-R2) whose lower boundary was imposed as a zero-concentration gradient. The continuous differential equations in equations (1) and (2) were solved using finite differences and the method-of-lines over an uneven grid with a higher spatial resolution at the surface and lower resolution towards the bottom. The model was solved using the NDSolve object of MATHEMATICA version 9.0. All simulations were run for long enough to achieve the steady state with a mass conservation of >99%. Parameter information and reaction terms of all species used in the model can be found in Table S2, Table S3, and Table S4.

3.4. Spatial Interpolation. Site-specific fluxes and rates were then used to explore area-based distribution in spatial coordinates by using the ordinary Kriging method. It is more accurate and realistic in this method to predict variables in the confined zone combining spatial distance with coordinate. According to Matheron [51], the mathematical principle of this method can be described as

$$Z'(x_0) = \sum_{i=1}^n \lambda_i Z(x_i), \quad (18)$$

where $Z(x_i)$ is a value which is situated at any place of the study area, x_0 is the predicted site, and λ_i is the weight factor, of which the sum is always equal to unity.

Spatial interpolation was implemented by ARCMAP version 10.5. Interpolation extent was derived by the point feature. The cell size of the output raster which was automatically created was 1/250 of the width and height of the extent.

4. Results

4.1. Porewater Geochemistry. We analysed 37 sediment cores, including 10 in Dongsha, 3 in Xisha, and 24 in Shenhu, and all the geochemical data are shown in Figure S1.

The sulfate concentration profiles in Dongsha generally show quasilinear depletion with depth. Especially in 2013DS-F, 2014DS-G4, and 2015DS17, sulfate concentrations show sharper decline towards the sulfate-methane transition zone (SMTZ) compared with those in other sites. Calcium concentration profiles in Dongsha display linear decline with depth. In contrast, DIC concentration profiles in Dongsha generally mirror the calcium concentration profiles.

The sulfate concentrations in Shenhu basically quasilinearly decline with depth but their gradients differ among sites. Similar to the calcium concentration profiles in Dongsha, calcium concentration profiles in Shenhu display linear decrease with depth and DIC concentration profiles show quasi-linear increase with depth.

The sulfate concentration profiles in Xisha do not follow the general trend of quasi-linear decrease. Instead, they show kink-type features with inflection points being located at 2 mbsf to 7 mbsf. The SO_4^{2-} concentrations in 2015XS-50 and 2015XS-R2 display near-seawater values in the upper 3-5 meters and then decline sharply towards the SMTZ. The seawater intrusion feature is also reflected by calcium concentration profiles, which is attributed to the irrigation of porewater caused by gas bubbling as demonstrated by previous studies [26, 52, 53]. At core 2015XS-44, the sulfate concentration profile does not show the feature of bubble irrigation but the calcium concentration profile still exhibits a kink at ~5 mbsf. The reason is not well understood at this moment, but it might be related to carbonate dissolution induced by organoclastic aerobic oxidation. At cores 2015XS-50 and 2015XS-R2, DIC concentration profiles also show the bubble irrigation feature and generally mirror the trend of sulfate concentration profiles.

4.2. Reaction-Transport Modeling. The simulation results for the three areas mostly reproduced the measured profiles. Model parameters used to constrain the model curve are listed in Table S2 and Table S3. In this model, phosphate concentration profiles were used to constrain the initial age of POC. Due to the lack of phosphate concentration profiles in the cores of Dongsha, initial ages in Dongsha (5000 yr) were adopted from Hu et al. [54]. For the same reason, the initial ages of 2015XS-44 and 2015XS-50 in Xisha were assumed to be the same as that of 2015XS-R2 derived from a measured phosphate concentration profile. Likewise, in the Shenhu area, the average initial age of TOC for the cores with phosphate data (200 ka) was taken to model those cores that lack phosphate sites. The modeled POC degradation rates are $11.2\text{-}24.5 \text{ mmol}\cdot\text{m}^{-2}\cdot\text{yr}^{-1}$ in Dongsha, $2.9\text{-}7.5 \text{ mmol}\cdot\text{m}^{-2}\cdot\text{yr}^{-1}$ in Xisha, and $7.2\text{-}30.7 \text{ mmol}\cdot\text{m}^{-2}\cdot\text{yr}^{-1}$ in Shenhu.

The depth-integrated rates and fluxes for the individual core are presented in Table S1. The rates of AOM in Dongsha range from 8.3 to $37.5 \text{ mmol}\cdot\text{m}^{-2}\cdot\text{yr}^{-1}$, which are similar to AOM rates in Shenhu (9.4 to $30.5 \text{ mmol}\cdot\text{m}^{-2}\cdot\text{yr}^{-1}$).

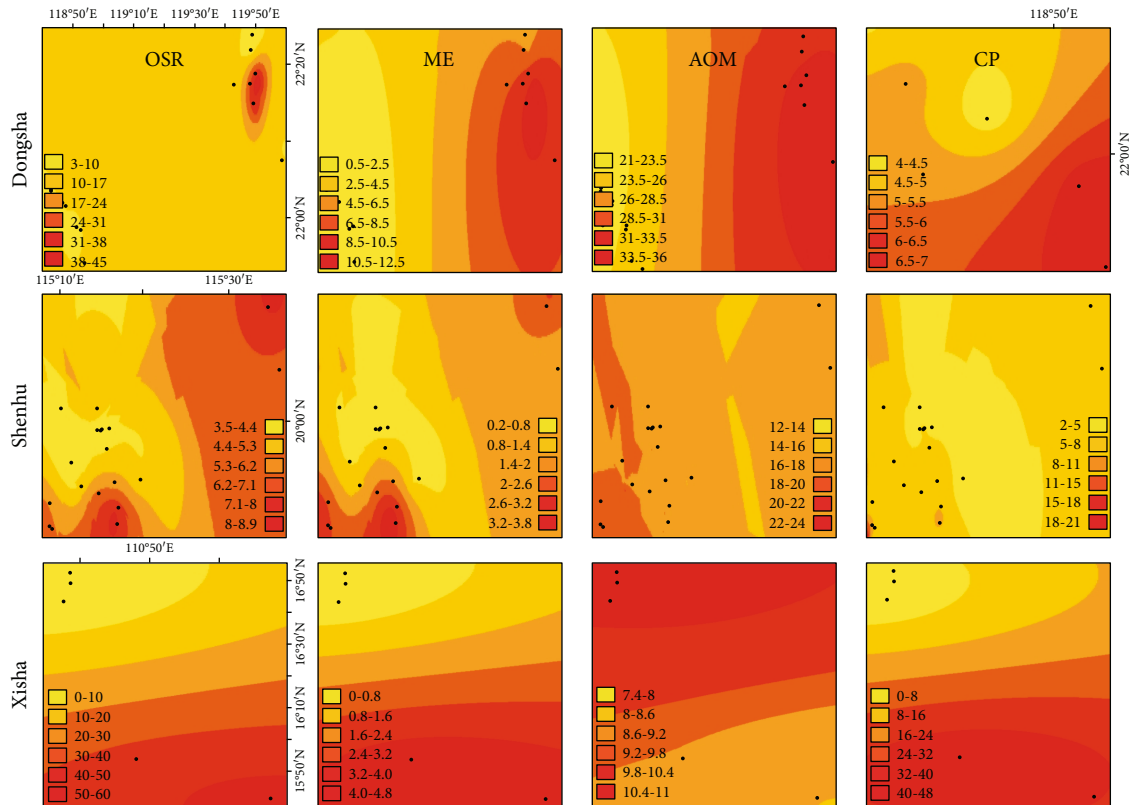


FIGURE 2: Spatial distribution of rates of organoclastic sulfate reduction (OSR), anaerobic oxidation of methane (AOM), methanogenesis (ME), and authigenic carbonate precipitation (CP) in the three areas. The black dots represent spatial distribution of sampling sites. Different colors denote different ranges of biogeochemical rates. In comparison to the interpolation rates of OSR, ME, and AOM in Dongsha, a smaller area was confined in the interpolation rate of CP. Additionally, rates of OSR, ME, AOM, and CP have the same interpolation region and so do those in Xisha.

In contrast, AOM rates in Xisha ($12.4\text{--}170.6\text{ mmol}\cdot\text{m}^{-2}\cdot\text{yr}^{-1}$) are greatly higher than those in Dongsha and Shenhu, because AOM was primarily supplied by methane gas dissolution. The methane fluxes at the top of the simulated sediment column are $0.002\text{--}0.2\text{ mmol}\cdot\text{m}^{-2}\cdot\text{yr}^{-1}$ in Dongsha, $0.002\text{--}0.3\text{ mmol}\cdot\text{m}^{-2}\cdot\text{yr}^{-1}$ in Shenhu, and $0.01\text{--}399.2\text{ mmol}\cdot\text{m}^{-2}\cdot\text{yr}^{-1}$ in Xisha. DIC fluxes in all three areas are approximately three to four orders of magnitude higher than methane fluxes with $13.1\text{--}26.1\text{ mmol}\cdot\text{m}^{-2}\cdot\text{yr}^{-1}$ in Dongsha, $10.1\text{--}31.7\text{ mmol}\cdot\text{m}^{-2}\cdot\text{yr}^{-1}$ in Shenhu, and $1\text{--}155\text{ mmol}\cdot\text{m}^{-2}\cdot\text{yr}^{-1}$ in Xisha. Rates of carbonate precipitation in Dongsha ($4.3\text{--}7.3\text{ mmol}\cdot\text{m}^{-2}\cdot\text{yr}^{-1}$), Shenhu ($3.6\text{--}9\text{ mmol}\cdot\text{m}^{-2}\cdot\text{yr}^{-1}$), and Xisha ($4.1\text{--}12.4\text{ mmol}\cdot\text{m}^{-2}\cdot\text{yr}^{-1}$) are comparable.

4.3. Spatial Interpolation. Interpolation was utilized to explore the spatial distribution of the biogeochemical rates of 395 cores, of which 37 cores are new in this study (see Table S1) and 358 cores were collected from literatures (see Table S5). As shown in Figure 2, rates of POC degradation via sulfate reduction and methanogenesis in Dongsha generally show high values in the east and gradually decrease towards the west. The rates of authigenic carbonate precipitation are mostly in agreement with those of AOM with higher values towards the east even though within a smaller region. The POC degradation rates in Xisha decrease from the south to the north. In contrast to that in the Dongsha area, the

distribution of AOM rates in the Xisha area is inconsistent with that of carbonate precipitation rates. This may be due to the lack of coordinates in some cores with high carbonate precipitation rates which are not incorporated in the north. Unlike the POC decomposition rate distribution in Dongsha and Xisha, two spots of intensified POC decomposition are located to the northeast and to the southwest in Shenhu. Rates of AOM and carbonate precipitation are generally low in the whole area.

5. Discussion

5.1. Regional Biogeochemical Rates and Fluxes of Methane and DIC. By upscaling the rates and fluxes in the specific sites into a region of interest, raster means were obtained by ARCMAP based on the small subareas divided automatically, which represent areal means. To better constrain the areal mean values of individual biogeochemical reactions in each area, we averaged arithmetical mean and raster mean values (see Table 1). Among the three areas, standard deviations of arithmetical means in the Xisha area were generally higher than 100, which indicate high heterogeneity of the biogeochemical rates. The arithmetical average of the rates of AOM in the Xisha area was much greater than those in the other two areas due to intensive methane bubbling. However, the raster mean of AOM rates in Xisha was slightly lower

TABLE 1: Biogeochemical rates and effluxes of methane and DIC in the three areas.

Location	CH ₄ efflux			DIC efflux			OSR			ME			AOM			CP			Cores						
	RM	AM	SD	Average	RM	AM	SD	Average	RM	AM	SD	Average	RM	AM	SD	Average	RM	AM		SD	Average				
Dongsha	0.2	9.7	95	4.9	25.3	19.3	7	22.3	14.1	17.7	12	15.9	5.1	4.8	4	4.9	29.0	26.7	14	27.8	5.5	5.4	1	5.3	363
Xisha	0.1	144	366	72	36.0	246.2	136	141	27.6	14.6	20	21.1	2.6	1.5	1	2	9.4	261.1	385	135.2	27.3	37.4	28	32.3	8
Shenhu	0.0	0.1	1	0.0	17.1	19.8	5	18.4	5.8	9.8	2	7.8	1.4	2.8	1	2.1	16.8	18.2	5	17.5	5.4	6.3	1.6	5.8	24
North SCS	0.13	11.3	96	5.7	29.5	62.9	178	46.2	19.6	13.4	12	16.5	3.6	3.2	3	3.4	19.0	60.8	180	39.9	15.4	12	17	13.7	395

RM: raster mean; AM: arithmetical mean; SD: standard deviation.

TABLE 2: Areal comparison of biogeochemical rates and effluxes of methane and DIC with other cold seeps.

Location	CH ₄ efflux	DIC efflux	OSR	ME	AOM	CP	Reference
Northern SCS	5.7	46.2	16.5	3.4	39.9	13.7	This study
Hydrate Ridge	839.5	9000		51.83	6575		[60, 68, 69]
Gulf of Mexico	109.5				1718		[73]
Costa Rica	4562.5				5880		[59]
Black Sea	3017				11363		[61]
Blake Ridge			2.92	0.365	10.6		[37]
Sakhalin Island (Derugin Basin)			59.9	11.9	33.2	11	[37]
Skagerrak (Denmark)	36.5				62		[70]
Hikurangi Margin (New Zealand)	4380	5548	2.5	1.5	333		[53, 58]
Ulleung Basin			23	53.8	40	6.3	[71, 72]
Vestnesa Ridge			12.8		184.8		[74]

than those at the other two areas. The inconsistent result derived using two different methods is ascribed to the exclusion of intensive seepage sites due to unavailability of the sampling locations from the interpolation. Regardless of all the discrepancies between the two methods, a tentative comparison among the three regions indicates that the rates of AOM and carbonate precipitation in Xisha are overwhelmingly larger than those in the other two areas and that the rate of organic matter degradation in Xisha was slightly higher than those in Dongsha and Shenhu areas. The low rates of biogeochemical reactions in Shenhu are likely due to the absence of methane seepage and the occurrence of deep-seated hydrates [12]. The Dongsha area always shows the intermediate rates compared with the other two areas owing to the occurrence of sporadic methane seepage sites and gas hydrates in shallow sediments.

The Xisha area is characterized by high content of sedimentary organic matter (up to 2%) mainly sourced from marine algae [55, 56]. This may explain the relatively higher rate of organic matter degradation in Xisha compared to Dongsha and Shenhu. Applying the bimolecular kinetics to calculate the AOM rate, we assume that the adjustable rate constant (k_{AOM}) represents the integrated effects of a number of factors including the microbial community structure and abundance, bioenergetics, and enzyme kinetics. Therefore, different settings may have distinct rate constants, ranging over 6 orders of magnitude [57]. Similar to the other passive continental margin environments, the rate constant ($k_{\text{AOM}} = 1$) in this study is generally lower than those in active continental margin environments [26, 37, 58–61]. In the cold seeps and hydrate-bearing area, methane expulsion is usually associated with some specific structures, e.g., mud diapir, fault, and gas chimney. These structures provide conduits for the upward migration of methane-rich fluid. According to the geophysical imaging in Dongsha, large amounts of mud diapir and gas chimney are well developed in subsurface sediments [62]. Gas bubble release was indicated by hydroacoustic flares, and indeed, gas ebullition was observed during ROV investigation [21, 63]. In the Shenhu area, acoustic blank in shallow horizons, presumably caused by the dissociation of deep-seated hydrates, is connected with the gas

chimney [64, 65]. The derived AOM rate in Shenhu ($17.5 \text{ mmol}\cdot\text{m}^{-2}\cdot\text{yr}^{-1}$) is consistent with a pioneer work ($20.9 \text{ mmol}\cdot\text{m}^{-2}\cdot\text{yr}^{-1}$ and $11 \text{ mmol}\cdot\text{m}^{-2}\cdot\text{yr}^{-1}$) [27, 66]. In the Xisha area, gas chimneys, pockmarks, and gas bubble as well as chemosynthesis-based biota were also observed [32, 67]. These observations are consistent with the porewater profiles showing a bubble irrigation feature and shallow SMTZ in the Xisha area. The authigenic carbonate precipitation is due to the DIC production by AOM, resulting in the highest rate of carbonate precipitation in Xisha.

Synthetic biogeochemical rates and fluxes of methane and DIC in the cold seeps and hydrate-bearing area of the northern SCS are also estimated by combining raster means of the three regions and arithmetical means of all the cores. In the northern SCS, area-based biogeochemical rates and fluxes of CH₄ and DIC were far lower than estimates only based on few single points in the other regions (see Table 2). In the active continental margins, e.g., Hydrate Ridge, Costa Rica, and Hikurangi Margin, strong tectonic compression and structural fractures generally facilitate the ascension of internal methane-rich fluid across the sediment-seawater interface. Therefore, the rates of AOM and the fluxes of methane and DIC in the three areas are uniformly at least two orders of magnitude higher than those in the northern SCS [53, 58–60, 68, 69]. In the passive continental margins, e.g., Blake Ridge, Sakhalin Island, Skagerrak, and Ulleung Basin, AOM rates and fluxes of methane and DIC in the other regions worldwide are comparable with those in the northern SCS [37, 61, 70–72]. With the exception of the Gulf of Mexico and Vestnesa Ridge, the extraordinarily high AOM rates and the flux of methane can be attributed to cores retrieved near the gas chimney in the Gulf of Mexico [73] and around the pockmark in the Vestnesa Ridge [74]. As the world's largest anoxic basin and the largest surface reservoir of aqueous methane, the Black Sea was known for its extremely high AOM rate and methane flux compared with the northern SCS [61]. Additionally, recent works have revealed that the AOM rate in marine sediments worldwide is $\sim 7.9\text{--}10.7 \text{ mmol}\cdot\text{m}^{-2}\cdot\text{yr}^{-1}$ [75], which is less than the rate ($39.9 \text{ mmol}\cdot\text{m}^{-2}\cdot\text{yr}^{-1}$) in the cold seep area of the northern South China Sea.

5.2. DIC and Aqueous Methane Turnover in the Shallow Sediments. Generally, the sources of DIC in cold seeps include OSR, AOM, and methanogenesis, whereas the major DIC sinks are carbonate precipitation and diffusive loss towards the bottom water [76, 77]. The relative contributions of the 5 processes mentioned above influencing the DIC pool in Dongsha, Xisha, Shenhu, and all cold seep sites in the northern SCS were shown in Figure 3. The three areas and the northern SCS exhibit similar patterns in terms of the sources and sinks of DIC pool. As for the sources of DIC, the contributions of each reaction to DIC production decrease in the order of AOM, OSR, and ME, with AOM accounting for more than 60% of the DIC production in all the three areas. This trend in the SCS is inconsistent with that in the Ulleung basin (AOM > ME > OSR), probably as a result of the difference in the reactivity of organic matter and modelled depth [71]. As for sinks of DIC, the fluxes of DIC towards the seafloor accounted for more than 80% of DIC sinks in all the areas and the authigenic carbonate precipitation only occupied about 20% of DIC sinks. Differences between sources and sinks in the three regions and northern SCS are $6.1 \text{ mmol}\cdot\text{m}^{-2}\cdot\text{yr}^{-1}$ in Dongsha, $17 \text{ mmol}\cdot\text{m}^{-2}\cdot\text{yr}^{-1}$ in Xisha, $2.7 \text{ mmol}\cdot\text{m}^{-2}\cdot\text{yr}^{-1}$ in Shenhu, and $5.9 \text{ mmol}\cdot\text{m}^{-2}\cdot\text{yr}^{-1}$ in the northern SCS. Even though mass conservations are kept in each modeling exercise, the imbalance in DIC may be attributed to the inclusion of numerous published calculations (see Table S5).

There are four major factors, including methanogenesis, AOM, diffusive migration of methane, and phase transformation, that constrain methane cycling in shallow sediments. In Dongsha and Shenhu, AOM consumed a vast majority of methane moving up towards the seafloor. In contrast, AOM only consumed ~65% of methane and the residual was transported towards the seafloor in Xisha. As for the source of methane, bubble dissolution can widely take place if the dissolved methane concentration is lower than its phase equilibrium concentration [39]. In Xisha, bubble dissolution (99%) played a predominant role in methane supply and methanogenesis barely accounted for 1% of methane sources. However, constant diffusive supply of methane from the lower boundary provided the major source of methane in Dongsha and Shenhu. The diffusive migration of methane accounted for 47% and 82% of the methane source in Dongsha and Shenhu, respectively. Additionally, the methanogenesis played a similar role in supplying methane to the sediments (17% in Dongsha and 12% in Shenhu).

5.3. Influence of Shallow Carbon Cycling on the Carbon Reservoir of Seawater. As essential components of long-term carbon cycle, the confluence of organic carbon burial, organic matter degradation, and AOM mediates the carbon equilibrium between seawater reservoir and deep carbon and persistently affects the ocean environment [78]. Organic materials of both terrestrial and marine in origin undergo microbial decomposition during settling, and less than 1% of organic matter from the surface ocean reaches the seafloor [79]. Following the aerobic and anaerobic oxidation of organic matter in the sediments, the remaining refractory

organic matter is permanently buried. According to the model results in each site, average POC burial flux below 20 mbsf is $186 \text{ mmol}\cdot\text{m}^{-2}\cdot\text{yr}^{-1}$ in the cold seeps and hydrate-bearing area of the northern SCS, which means that 2.8 Gmol POC are buried annually (see Figure 4). As the final step of the organic matter, methanogenesis produces both methane and some other dissolved organic matters (DOM), e.g., formate and acetate [80]. The majority of methane is consumed by AOM, thereby generating DIC as the byproduct. The remaining methane and other DOM may migrate towards the sediment-water interface [81].

As we mentioned above, carbon entering the seawater from the sediments in the form of DIC and DOM can also, to some extent, influence the deep ocean carbon cycling, especially the carbonate saturation state in the water column [82, 83]. In the hydrate-bearing area of the northern SCS, DOM effluxes in the form of aqueous methane were $\sim 5 \text{ mmol}\cdot\text{m}^{-2}\cdot\text{yr}^{-1}$ (see Figure 4). By multiplying by the area of $1.6 \times 10^4 \text{ km}^2$, $9 \times 10^{-5} \text{ Tmol}$ aqueous methane is released out of the sediments annually. Irrespective of gaseous methane in the intensive gas seepage sites, such considerable amounts of DOM diffusing towards the bottom water may play an important role in the DOM cycling in the deep waters of the northern SCS. Recent studies have shown much greater DOM fluxes ($0.1 \text{ mol}\cdot\text{m}^{-2}\cdot\text{yr}^{-1}$) by accounting for other forms of DOM species such as volatile fatty acids [80, 83]. Thus, the widely distributed gas hydrates and cold seeps in the northern SCS could contribute far more than $9 \times 10^{-5} \text{ Tmol DOM/yr}$ to the ocean if gaseous methane and other organic acids are incorporated into the flux calculation. Additionally, DIC efflux ($46 \text{ mmol}\cdot\text{m}^{-2}\cdot\text{yr}^{-1}$) was several times higher than dissolved methane flux. Similarly, multiplying it by the area of cold seeps and hydrate-bearing areas gives an annual release amount of $7 \times 10^{-4} \text{ Tmol}\cdot\text{C}\cdot\text{yr}^{-1}$. Despite that this estimation is not comparable to the DIC flux on the shelf [84], it may have an impact on the bottom water chemistry in cold seeps and hydrate-bearing areas. Release of DIC into bottom water can, in some case, prompt the production and preservation of biogenic and authigenic carbonate. Nevertheless, aerobic oxidation of methane released from sediments produces CO_2 and lowers the seawater pH, thereby probably dissolving carbonate [82]. Accordingly, a total of $8.2 \times 10^{-4} \text{ Tmol}$ dissolved carbon is released into bottom water annually but its influence on bottom water carbonate systems is still unclear.

6. Conclusion

This study is aimed at quantitatively assessing the carbon turnover within the shallow sediments and quantifying the areal effluxes of methane and DIC in Xisha, Dongsha, and Shenhu, northern SCS. A 1-D reaction-transport model was used to calculate the biogeochemical rates and fluxes of methane and DIC in the 37 new collected cores. In addition, a total of 395 cores, including 358 cores reported in pioneer literatures, were used to extrapolate the areal rates and fluxes by spatial interpolation in the northern SCS. The average of the arithmetical mean and interpolation mean revealed that

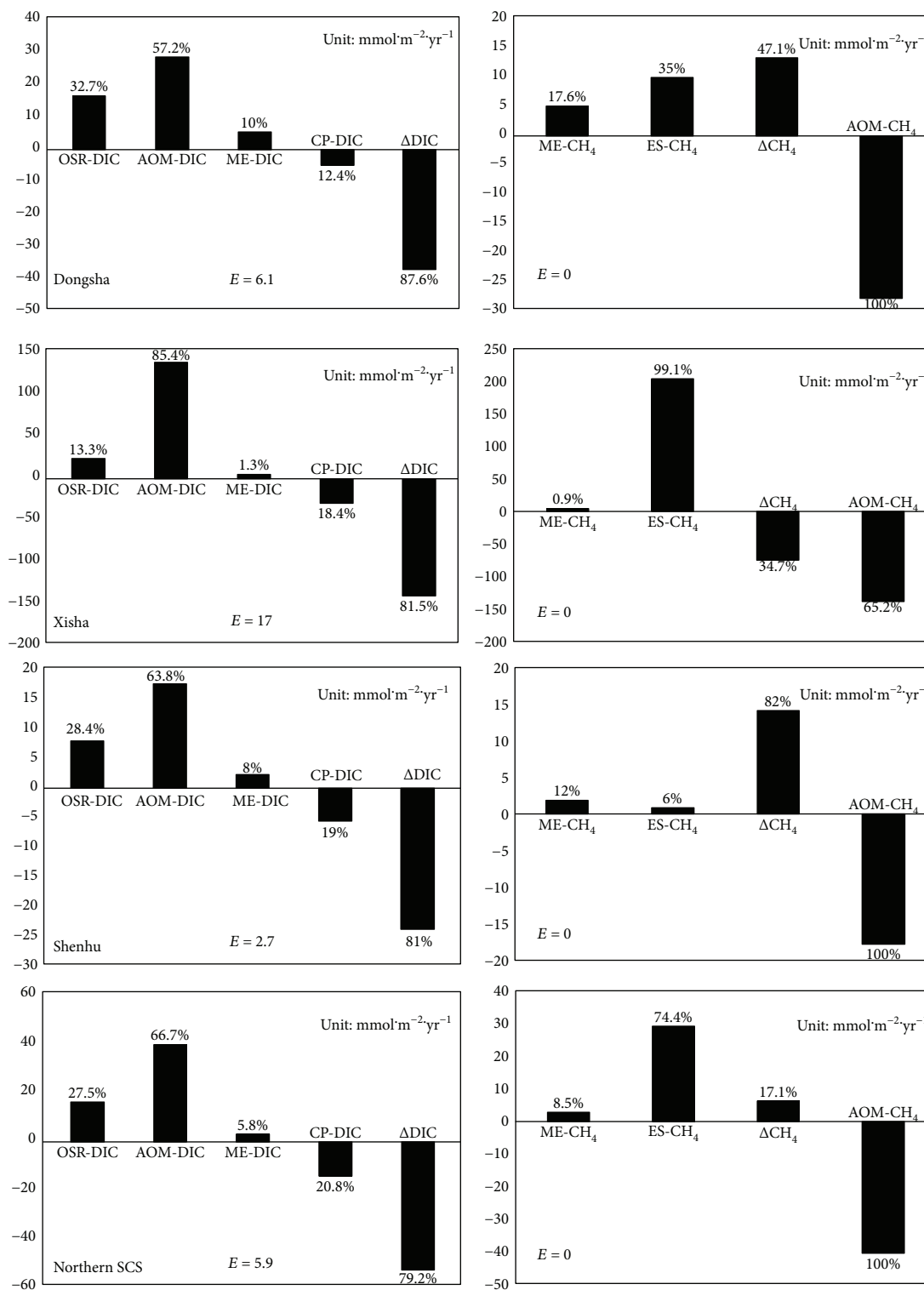


FIGURE 3: Sources and sinks of methane and DIC in the shallow sediments. Positive values denote sources of methane or DIC and negative values denote sinks of methane or DIC. OSR: organoclastic sulfate reduction; AOM: anaerobic oxidation of methane; ME: methanogenesis; CP: carbonate precipitation; ES: external methane from the bubble dissolution within modeled sediment columns. Δ represents difference between fluxes at the lower boundary and fluxes at the upper boundary. Percentages above or below each column represent the contributions of each biogeochemical reaction to the source/sink. E denotes the differences between sources and sinks of methane and DIC. Biogeochemical rates (OSR, AOM, ME, and CP) in the three regions and northern SCS are adopted from Table 1. The ES-CH₄ was obtained by assuming a complete mass conservation of methane.

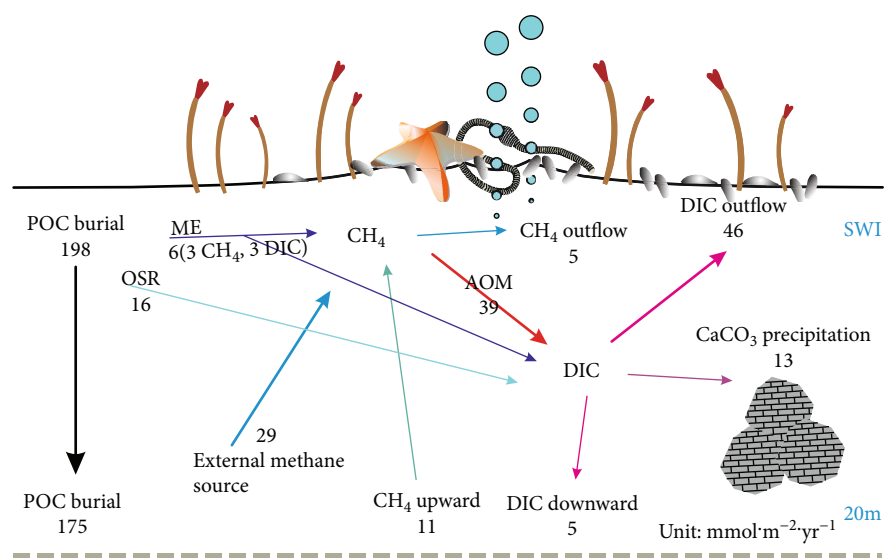


FIGURE 4: Shallow carbon cycling in the cold seeps and gas hydrate-bearing sediments in the northern South China Sea. The numbers in bold represent mean values of interpolation mean and arithmetic mean (Table 1). The numbers in italic are derived from the model. The number in grey is estimated considering methane mass conservation.

the rates of AOM and carbonate precipitation and effluxes of methane and DIC in Xisha were at least one order of magnitude higher than those in Dongsha and Shenhu and the rate of organic matter degradation in Xisha was slightly higher than those in the other two areas. This is because of the occurrence of intensive methane gas bubbling in Xisha. However, the diffusive source played the predominant role in methane supply in the other two areas. The majority of DIC mainly produced by AOM is diffused out of sediments in the three areas. In comparison to those in the active continental margin and euxinic environment, the AOM rates and fluxes of methane and DIC in the cold seeps of the northern SCS were much lower. Alternatively, source and sink analysis of methane revealed that the bubble dissolution in Xisha contributed most of the methane. According to the estimates in this study, ~2.8 Gmol organic matter was buried and at least ~0.8 Gmol dissolved carbon was released from marine sediments annually. Nonetheless, to what extent the impact of carbon release from the shallow sediments on the oceanic carbon reservoir remains to be investigated.

Data Availability

Data used in this article can be obtained upon request via the email address zhangyanping@gig.ac.cn.

Conflicts of Interest

The authors declare that there is no conflict of interest regarding the publication of this paper.

Acknowledgments

This study was supported by the National Key R&D Program of China (2018YFC0310003), National Natural Science Fund of China (Grant nos. 41730528 and 91228206),

and China Geological Survey project (DD20189310). We thank the crews of RVs Haiyang-4 and Shiyan-3 for their help with sampling at sea.

Supplementary Materials

There are 5 tables and 1 figure in the supplementary material. In Table S1, core length, water depth, sampling tools, and outputs of the reaction-transport models of the new 37 cores in this paper are listed. The fixed parameters and fitted parameters used in the reaction-transport models at the 37 sites are listed in Table S2 and Table S3. In the reaction-transport model, concentrations of every species modelled are constrained by biogeochemical reactions within the model depth in addition to physical transport processes. Each reaction term of all species is listed in Table S4. Figure S1 detailed the concentration depth profiles of the 37 cores and displayed the curve of model output. All those mentioned above are the detailed description of the reaction-transport model. Data listed in Table S5 are collected from pioneer works, which contribute to the subsurface carbon cycling assessment of the study areas in Table 1 of the manuscript. (*Supplementary Materials*)

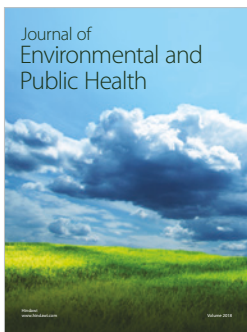
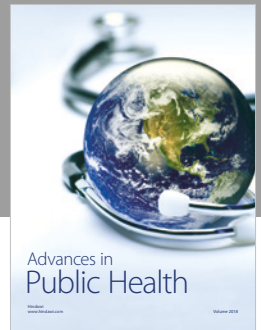
References

- [1] B. Buffett and D. Archer, "Global inventory of methane clathrate: sensitivity to changes in the deep ocean," *Earth and Planetary Science Letters*, vol. 227, no. 3-4, pp. 185-199, 2004.
- [2] K. A. Kvenvolden, "Gas hydrates-geological perspective and global change," *Reviews of Geophysics*, vol. 31, no. 2, pp. 173-187, 1993.
- [3] K. Wallmann, E. Pinero, E. Burwicz et al., "The global inventory of methane hydrate in marine sediments: a theoretical approach," *Energies*, vol. 5, no. 7, pp. 2449-2498, 2012.

- [4] A. V. Milkov, "Global estimates of hydrate-bound gas in marine sediments: how much is really out there?," *Earth-Science Reviews*, vol. 66, no. 3-4, pp. 183–197, 2004.
- [5] Y. Cao, D. Chen, and L. M. Cathles, "A kinetic model for the methane hydrate precipitated from venting gas at cold seep sites at Hydrate Ridge, Cascadia margin, Oregon," *Journal of Geophysical Research: Solid Earth*, vol. 118, no. 9, pp. 4669–4681, 2013.
- [6] D. F. Chen, Y. Y. Huang, X. L. Yuan, and L. M. Cathles III, "Seep carbonates and preserved methane oxidizing archaea and sulfate reducing bacteria fossils suggest recent gas venting on the seafloor in the Northeastern South China Sea," *Marine and Petroleum Geology*, vol. 22, no. 5, pp. 613–621, 2005.
- [7] Z. Duan, N. Møller, J. Greenberg, and J. H. Weare, "The prediction of methane solubility in natural waters to high ionic strength from 0 to 250°C and from 0 to 1600 bar," *Geochimica et Cosmochimica Acta*, vol. 56, no. 4, pp. 1451–1460, 1992.
- [8] E. Suess, "Marine cold seeps and their manifestations: geological control, biogeochemical criteria and environmental conditions," *International Journal of Earth Sciences*, vol. 103, no. 7, pp. 1889–1916, 2014.
- [9] A. Boetius, K. Ravensschlag, C. J. Schubert et al., "A marine microbial consortium apparently mediating anaerobic oxidation of methane," *Nature*, vol. 407, no. 6804, pp. 623–626, 2000.
- [10] K. Knittel and A. Boetius, "Anaerobic oxidation of methane: progress with an unknown process," *Annual Review of Microbiology*, vol. 63, no. 1, pp. 311–334, 2009.
- [11] D.-F. Chen, X.-X. Li, and B. Xia, "Distribution features of gas hydrate stable zones and resource prediction of the Qiongdongnan basin in the South China Sea," *Chinese Journal of Geophysics*, vol. 47, no. 3, pp. 548–555, 2004.
- [12] Y. Shengxiong, Z. Ming, L. Jinqiang et al., "Preliminary results of China's third gas hydrate drilling expedition: a critical step from discovery to development in the South China Sea," *Fire in the Ice*, vol. 15, no. 2, 2015.
- [13] G. X. Zhang, S. X. Yang, M. Zhang et al., "GMGS2 expedition investigates rich and complex gas hydrate environment in the South China Sea," *Center for Natural Gas and Oil*, vol. 412, pp. 386–7614, 2014.
- [14] H. Q. Zhang, S. Yang, N. Wu et al., "Successful and surprising results for China's first gas hydrate drilling expedition," *Fire in the Ice*, vol. 9, 2007.
- [15] H. Deng, P. Yan, H. Liu, and W. Luo, "Seismic data processing and the characterization of a gas hydrate bearing zone offshore of southwestern Taiwan," *Terrestrial, Atmospheric and Oceanic Sciences*, vol. 17, no. 4, pp. 781–797, 2006.
- [16] J. Feng, S. Yang, J. Liang et al., "Methane seepage inferred from the porewater geochemistry of shallow sediments in the Beikang Basin of the southern South China Sea," *Journal of Asian Earth Sciences*, vol. 168, pp. 77–86, 2018.
- [17] G. Hui, S. Li, L. Guo et al., "Source and accumulation of gas hydrate in the northern margin of the South China Sea," *Marine and Petroleum Geology*, vol. 69, pp. 127–145, 2016.
- [18] X. Wang, N. Li, D. Feng et al., "Using chemical compositions of sediments to constrain methane seepage dynamics: a case study from Haima cold seeps of the South China Sea," *Journal of Asian Earth Sciences*, vol. 168, pp. 137–144, 2018.
- [19] S. Wu, G. Zhang, Y. Huang, J. Liang, and H. K. Wong, "Gas hydrate occurrence on the continental slope of the northern South China Sea," *Marine and Petroleum Geology*, vol. 22, no. 3, pp. 403–412, 2005.
- [20] P. Yan, H. Deng, and H. Liu, "The geological structure and prospect of Gas Hydrate over the Dongsha Slope, South China Sea," *Terrestrial, Atmospheric and Oceanic Sciences*, vol. 17, no. 4, pp. 645–658, 2006.
- [21] D. Feng, M. Cheng, S. Kiel et al., "Using *Bathymodiolus* tissue stable carbon, nitrogen and sulfur isotopes to infer biogeochemical process at a cold seep in the South China Sea," *Deep Sea Research Part I: Oceanographic Research Papers*, vol. 104, pp. 52–59, 2015.
- [22] X. Han, E. Suess, Y. Huang et al., "Jiulong methane reef: microbial mediation of seep carbonates in the South China Sea," *Marine Geology*, vol. 249, no. 3-4, pp. 243–256, 2008.
- [23] Z. Lin, X. Sun, J. Peckmann et al., "How sulfate-driven anaerobic oxidation of methane affects the sulfur isotopic composition of pyrite: a SIMS study from the South China Sea," *Chemical Geology*, vol. 440, pp. 26–41, 2016.
- [24] M. Luo, L. Chen, S. Wang, W. Yan, H. Wang, and D. Chen, "Pockmark activity inferred from pore water geochemistry in shallow sediments of the pockmark field in southwestern Xisha Uplift, northwestern South China Sea," *Marine and Petroleum Geology*, vol. 48, pp. 247–259, 2013.
- [25] H. Tong, D. Feng, H. Cheng et al., "Authigenic carbonates from seeps on the northern continental slope of the South China Sea: new insights into fluid sources and geochronology," *Marine and Petroleum Geology*, vol. 43, pp. 260–271, 2013.
- [26] P.-C. Chuang, A. W. Dale, K. Wallmann et al., "Relating sulfate and methane dynamics to geology: accretionary prism offshore SW Taiwan," *Geochemistry, Geophysics, Geosystems*, vol. 14, no. 7, pp. 2523–2545, 2013.
- [27] Y. Hu, M. Luo, L. Chen et al., "Methane source linked to gas hydrate system at hydrate drilling areas of the South China Sea: Porewater geochemistry and numerical model constraints," *Journal of Asian Earth Sciences*, vol. 168, pp. 87–95, 2018.
- [28] B. Taylor and D. E. Hayes, "Origin and history of the South China Sea Basin," *The Tectonic and Geologic Evolution of Southeast Asian Seas and Islands: Part 2*, vol. 27, pp. 23–56, 1983.
- [29] P. Clift and J. Lin, "Preferential mantle lithospheric extension under the South China margin," *Marine and Petroleum Geology*, vol. 18, no. 8, pp. 929–945, 2001.
- [30] X. Xie, R. D. Müller, S. Li, Z. Gong, and B. Steinberger, "Origin of anomalous subsidence along the northern South China Sea margin and Its relationship to dynamic topography," *Marine and Petroleum Geology*, vol. 23, no. 7, pp. 745–765, 2006.
- [31] Z. Sha, J. Liang, G. Zhang et al., "A seepage gas hydrate system in northern South China Sea: seismic and well log interpretations," *Marine Geology*, vol. 366, pp. 69–78, 2015.
- [32] Q. Liang, Y. Hu, D. Feng et al., "Authigenic carbonates from newly discovered active cold seeps on the northwestern slope of the South China Sea: constraints on fluid sources, formation environments, and seepage dynamics," *Deep Sea Research Part I: Oceanographic Research Papers*, vol. 124, pp. 31–41, 2017.
- [33] V. N. Ivanenkov and Y. I. Lyakhin, "Determination of total alkalinity in seawater," in *Methods of Hydrochemical Investigations in the Ocean*, O. K. Bordovsky and V. N. Ivanenkov, Eds., pp. 110–114, Nauka Publ, House, 1978.
- [34] Y. Hu, D. Feng, Q. Liang, Z. Xia, L. Chen, and D. Chen, "Impact of anaerobic oxidation of methane on the geochemical cycle of redox-sensitive elements at cold-seep sites of the northern South China Sea," *Deep Sea Research Part II: Topical Studies in Oceanography*, vol. 122, pp. 84–94, 2015.

- [35] R. A. Berner, *Early Diagenesis: A Theoretical Approach*, Princeton University Press, 1980.
- [36] B. P. Boudreau, *Diagenetic Models and Their Implementation*, Springer, 1997.
- [37] K. Wallmann, G. Aloisi, M. Haeckel, A. Obzhairov, G. Pavlova, and P. Tishchenko, "Kinetics of organic matter degradation, microbial methane generation, and gas hydrate formation in anoxic marine sediments," *Geochimica et Cosmochimica Acta*, vol. 70, no. 15, pp. 3905–3927, 2006.
- [38] L. Yuan-Hui and S. Gregory, "Diffusion of ions in sea water and in deep-sea sediments," *Geochimica et Cosmochimica Acta*, vol. 38, no. 5, pp. 703–714, 1974.
- [39] M. Haeckel, B. P. Boudreau, and K. Wallmann, "Bubble-induced porewater mixing: A 3-D model for deep porewater irrigation," *Geochimica et Cosmochimica Acta*, vol. 71, no. 21, pp. 5135–5154, 2007.
- [40] G. E. Claypool, A. V. Milkov, Y.-J. Lee, M. E. Torres, W. S. Borowski, and H. Tomaru, "Microbial methane generation and gas transport in shallow sediments of an accretionary complex, southern hydrate ridge (ODP leg 204), Offshore Oregon, USA," in *Proceeding of the Ocean Drilling Program, Scientific Results*, A. M. Tréhu, G. Bohrmann, M. E. Torres, and F. S. Colwell, Eds., pp. 1–52, Ocean Drilling Program, College Station, TX, USA, 2006.
- [41] H. D. Schulz and M. Zabel, *Marine Geochemistry*, Springer, Berlin, Germany, 2006.
- [42] M. Thullner, A. W. Dale, and P. Regnier, "Global-scale quantification of mineralization pathways in marine sediments: a reaction-transport modeling approach," *Geochemistry, Geophysics, Geosystems*, vol. 10, no. 10, 2009.
- [43] J. T. Westrich and R. A. Berner, "The role of sedimentary organic matter in bacterial sulfate reduction: the G model tested," *Limnology and Oceanography*, vol. 29, no. 2, pp. 236–249, 1984.
- [44] J. Middelburg, "A simple rate model for organic matter decomposition in marine sediments," *Geochimica et Cosmochimica Acta*, vol. 53, no. 7, pp. 1577–1581, 1989.
- [45] W. S. Reece, "Oceanic methane biogeochemistry," *Chemical Reviews*, vol. 107, no. 2, pp. 486–513, 2007.
- [46] G. Bohrmann, J. Greinert, E. Suess, and M. Torres, "Authigenic carbonates from the Cascadia subduction zone and their relation to gas hydrate stability," *Geology*, vol. 26, no. 7, pp. 647–650, 1998.
- [47] L. D. Kulm, E. Suess, J. C. Moore et al., "Oregon subduction zone: venting, fauna, and carbonates," *Science*, vol. 231, no. 4738, pp. 561–566, 1986.
- [48] F. J. Millero, "Thermodynamics of the carbon dioxide system in the oceans," *Geochimica et Cosmochimica Acta*, vol. 59, no. 4, pp. 661–677, 1995.
- [49] R. E. Zeebe and D. Wolf-Gladrow, *CO₂ in Seawater: Equilibrium, Kinetics, Isotopes*, Elsevier, 2001.
- [50] Z. Duan, N. Møller, and J. H. Weare, "An equation of state for the CH₄-CO₂-H₂O system: I. Pure systems from 0 to 1000°C and 0 to 8000 bar," *Geochimica et Cosmochimica Acta*, vol. 56, no. 7, pp. 2605–2617, 1992.
- [51] G. Matheron, "Principles of geostatistics," *Economic Geology*, vol. 58, no. 8, pp. 1246–1266, 1963.
- [52] M. Haeckel, E. Suess, K. Wallmann, and D. Rickert, "Rising methane gas bubbles form massive hydrate layers at the seafloor," *Geochimica et Cosmochimica Acta*, vol. 68, no. 21, pp. 4335–4345, 2004.
- [53] M. Luo, A. W. Dale, L. Haffert et al., "A quantitative assessment of methane cycling in Hikurangi Margin sediments (New Zealand) using geophysical imaging and biogeochemical modeling," *Geochemistry, Geophysics, Geosystems*, vol. 17, no. 12, pp. 4817–4835, 2016.
- [54] Y. Hu, L. Chen, D. Feng, Q. Liang, Z. Xia, and D. Chen, "Geochemical record of methane seepage in authigenic carbonates and surrounding host sediments: A case study from the South China Sea," *Journal of Asian Earth Sciences*, vol. 138, pp. 51–61, 2017.
- [55] M. Cao, Q. Ma, Y. Wu, and J. Zhang, "Difference in organic matter distribution and degradation in surface sediment between northern South China Sea and Hainan island," *Oceanologia et Limnologia Sinica*, vol. 48, pp. 258–265, 2017.
- [56] C.-Y. Huang, S.-F. Wu, M. Zhao et al., "Surface ocean and monsoon climate variability in the South China Sea since the last glaciation," *Marine Micropaleontology*, vol. 32, no. 1–2, pp. 71–94, 1997.
- [57] P. Regnier, A. W. Dale, S. Arndt, D. E. LaRowe, J. Mogollón, and P. van Cappellen, "Quantitative analysis of anaerobic oxidation of methane (AOM) in marine sediments: a modeling perspective," *Earth-Science Reviews*, vol. 106, no. 1–2, pp. 105–130, 2011.
- [58] A. W. Dale, S. Sommer, M. Haeckel et al., "Pathways and regulation of carbon, sulfur and energy transfer in marine sediments overlying methane gas hydrates on the Opuawe Bank (New Zealand)," *Geochimica et Cosmochimica Acta*, vol. 74, no. 20, pp. 5763–5784, 2010.
- [59] P. Linke, K. Wallmann, E. Suess, C. Hensen, and G. Rehder, "In situ benthic fluxes from an intermittently active mud volcano at the Costa Rica convergent margin," *Earth and Planetary Science Letters*, vol. 235, no. 1–2, pp. 79–95, 2005.
- [60] R. Luff and K. Wallmann, "Fluid flow, methane fluxes, carbonate precipitation and biogeochemical turnover in gas hydrate-bearing sediments at Hydrate Ridge, Cascadia Margin: numerical modeling and mass balances," *Geochimica et Cosmochimica Acta*, vol. 67, no. 18, pp. 3403–3421, 2003.
- [61] K. Wallmann, M. Drews, G. Aloisi, and G. Bohrmann, "Methane discharge into the Black Sea and the global ocean via fluid flow through submarine mud volcanoes," *Earth and Planetary Science Letters*, vol. 248, no. 1–2, pp. 545–560, 2006.
- [62] J. Shang, Z. Sha, J. Liang, and L. Wu, "Seep gas acoustic features and its indication to gas hydrate exploration on the slope of the northeastern South China Sea," *Georesearch of Ecological South China Sea*, no. 1, pp. 25–36, 2013.
- [63] C. Jiang-Xin, S. Hai-Bin, G. Yong-Xian, Y. Sheng-Xiong, B. Yang, and G. Ming-Hui, "A preliminary study of submarine cold seeps by seismic oceanography techniques," *Chinese Journal of Geophysics*, vol. 60, no. 1, pp. 117–129, 2017.
- [64] S. Li, F. Chu, Y. Fang, Z. Wu, and Y. Ni, "Associated interpretation of sub-bottom and single-channel seismic profiles from slope of Shenhu Area in the northern South China Sea—characteristics of gas hydrate sediment," *Journal of Tropical Oceanography*, vol. 29, no. 4, pp. 56–62, 2010.
- [65] Y. Ni, Y. Zheng, and S. Li, "Preliminary interpretation of a typical sub-bottom profile from the upper slope of Shenhu area in the northern South China Sea," *Journal of Marine Sciences*, vol. 27, pp. 30–36, 2009.
- [66] L. S. Wu, S. X. Yang, J. Q. Liang et al., "Variations of pore water sulfate gradients in sediments as indicator for underlying gas hydrate in Shenhu Area, the South China Sea," *Science China Earth Sciences*, vol. 56, no. 4, pp. 530–540, 2013.

- [67] X. Wang, S. Wu, D. Dong, Y. Guo, and H. Deborah, "Control of mass transport deposits over the occurrence of gas hydrate in Qiongdongnan basin," *Marine Geology & Quaternary Geology*, vol. 31, no. 1, pp. 109–118, 2011.
- [68] S. Sommer, O. Pfannkuche, P. Linke et al., "Efficiency of the benthic filter: biological control of the emission of dissolved methane from sediments containing shallow gas hydrates at Hydrate Ridge," *Global Biogeochemical Cycles*, vol. 20, no. 2, 2006.
- [69] T. Treude, A. Boetius, K. Knittel, K. Wallmann, and B. Barker Jørgensen, "Anaerobic oxidation of methane above gas hydrates at Hydrate Ridge, NE Pacific Ocean," *Marine Ecology Progress Series*, vol. 264, pp. 1–14, 2003.
- [70] A. W. Dale, P. Regnier, N. J. Knab, B. B. Jørgensen, and P. Van Cappellen, "Anaerobic oxidation of methane (AOM) in marine sediments from the Skagerrak (Denmark): II. Reaction-transport modeling," *Geochimica et Cosmochimica Acta*, vol. 72, no. 12, pp. 2880–2894, 2008.
- [71] W.-L. Hong, M. E. Torres, J.-H. Kim, J. Choi, and J.-J. Bahk, "Carbon cycling within the sulfate-methane-transition-zone in marine sediments from the Ulleung Basin," *Biogeochemistry*, vol. 115, no. 1-3, pp. 129–148, 2013.
- [72] J.-H. Kim, M.-H. Park, U. Tsunogai et al., "Geochemical characterization of the organic matter, pore water constituents and shallow methane gas in the eastern part of the Ulleung Basin, East Sea (Japan Sea)," *Island Arc*, vol. 16, no. 1, pp. 93–104, 2007.
- [73] W. Ussler III and C. K. Paull, "Rates of anaerobic oxidation of methane and authigenic carbonate mineralization in methane-rich deep-sea sediments inferred from models and geochemical profiles," *Earth and Planetary Science Letters*, vol. 266, no. 3-4, pp. 271–287, 2008.
- [74] W.-L. Hong, S. Sauer, G. Panieri et al., "Removal of methane through hydrological, microbial, and geochemical processes in the shallow sediments of pockmarks along eastern Vestnesa Ridge (Svalbard)," *Limnology and Oceanography*, vol. 61, no. S1, pp. S324–S343, 2016.
- [75] M. Egger, N. Riedinger, J. M. Mogollón, and B. B. Jørgensen, "Global diffusive fluxes of methane in marine sediments," *Nature Geoscience*, vol. 11, no. 6, pp. 421–425, 2018.
- [76] S. Chatterjee, G. R. Dickens, G. Bhatnagar et al., "Pore water sulfate, alkalinity, and carbon isotope profiles in shallow sediments above marine gas hydrate systems: A numerical modeling perspective," *Journal of Geophysical Research*, vol. 116, pp. 1–25, 2011.
- [77] W. S. Borowski, T. M. Hoehler, M. J. Alperin, N. M. Rodriguez, and C. K. Paull, "Significance of anaerobic methane oxidation in methane-rich sediments overlying the Black Ridge gas hydrates," in *Proceeding of the Ocean Drilling Programs, Scientific Results*, vol. 164, pp. 87–99, 2000.
- [78] R. A. Berner, *The Phanerozoic Carbon Cycle: CO₂ and O₂*, Oxford university press, New York, NY, USA, 2004.
- [79] A. Boetius and F. Wenzhöfer, "Seafloor oxygen consumption fuelled by methane from cold seeps," *Nature Geoscience*, vol. 6, no. 9, pp. 725–734, 2013.
- [80] V. B. Heuer, J. W. Pohlman, M. E. Torres, M. Elvert, and K.-U. Hinrichs, "The stable carbon isotope biogeochemistry of acetate and other dissolved carbon species in deep seafloor sediments at the northern Cascadia Margin," *Geochimica et Cosmochimica Acta*, vol. 73, no. 11, pp. 3323–3336, 2009.
- [81] J. W. Pohlman, J. E. Bauer, W. F. Waite, C. L. Osburn, and N. R. Chapman, "Methane hydrate-bearing seeps as a source of aged dissolved organic carbon to the oceans," *Nature Geoscience*, vol. 4, no. 1, pp. 37–41, 2011.
- [82] A. J. Andersson, F. T. Mackenzie, and L. M. Ver, "Solution of shallow-water carbonates: an insignificant buffer against rising atmospheric CO₂," *Geology*, vol. 31, no. 6, pp. 513–516, 2003.
- [83] C. W. Hung, K. H. Huang, Y. Y. Shih et al., "Benthic fluxes of dissolved organic carbon from gas hydrate sediments in the northern South China Sea," *Scientific Reports*, vol. 6, no. 1, article 29597, 2016.
- [84] V. Krumins, M. Gehlen, S. Arndt, P. Van Cappellen, and P. Regnier, "Dissolved inorganic carbon and alkalinity fluxes from coastal marine sediments: model estimates for different shelf environments and sensitivity to global change," *Biogeochemistry*, vol. 10, no. 1, pp. 371–398, 2013.



Hindawi

Submit your manuscripts at
www.hindawi.com

